scientific reports

Check for updates

OPEN

MOF enhances the sensitivity and selectivity of sorafenib as an anticancer drug against hepatocellular carcinoma and colorectal cancer in vitro

Emad M. ElZayat[1]✉, Nadeen M. Hassan[2], Rehab Mahmoud[3], Essam Ibrahim[4,5] & Nourhan Hassan[1]✉

Hepatocellular carcinoma (HCC) is the fifth most common cancer in the world and the second largest contributor to cancer mortality. Sorafenib (SOR) is a drug approved by the Food and Drug Administration (FDA) to treat liver cancer, but it has harsh side effects on normal cells, is expensive, and is associated with chemoresistance through frequent use. This work aims to test the hypothesis that loading sorafenib onto a metal-organic framework (MOF) as a nanocarrier can help increase the potency and selectivity of sorafenib on hepatocellular carcinoma (HCC) and explore its potential application in colorectal cancer treatment. MOFs were prepared and chemically characterized using XRD, FTIR, and BET. The crystallite size was calculated using the Scherrer equation, and comprehensive FTIR peak assignments were performed to elucidate drug-MOF interactions. Sorafenib was loaded onto the MOF, entrapment efficiency (EE) as well as loading capacity (LC) were calculated using the formulas: EE% = (sorafenib content loaded in MIL-53(Fe)) / (initial sorafenib content) × 100% and LC% = (sorafenib content loaded in MIL-53(Fe)) / (sorafenib loaded + weight of MIL-53(Fe)) × 100%, and in vitro release was evaluated under sink conditions in phosphate-buffered saline (PBS, pH 7.4). The cytotoxic effect of sorafenib on normal HFb-4, HepG2, and HCT-116 cells was measured before and after loading onto MOF, and the selectivity index (SI) was calculated using the formula: SI = IC_{50} (normal cells) / IC_{50} (cancer cells). Apoptosis and cell cycle analysis were also performed using flow cytometry. The present study showed entrapment efficiency (EE) = 88.97% and loading capacity (LC) = 23.5% of sorafenib. The high variability in LC indicates batch-to-batch reproducibility challenges that require optimization. Spontaneous release of the loaded drug was encountered within 48 h. XRD analysis showed crystallite sizes calculated using the Scherrer equation, confirming successful drug encapsulation with reduced crystallinity of sorafenib within the MOF structure. Before loading, the MTT test showed IC_{50} for sorafenib = 5.88, 12.5, 29.4 µg/ml on HFb-4, HepG2, and HCT-116 cells, respectively. After loading, IC_{50} values of 3.3, 5.5, and 7.9 µg/ml were found considering the loading capacity. The selectivity index (SI) values showed modest improvements: 0.46 to 0.6 for HepG2 and 0.2 to 0.42 for HCT-116. While these improvements are statistically significant, the SI values remain below the ideal threshold of > 2, indicating that further optimization is needed to achieve clinically relevant selectivity. There was a direct correlation between the cytotoxic effect and the degree of apoptosis in the HepG2 cell line. The present study has also proved cell cycle arrest at the G0/G1 phase after treatment with sorafenib loaded onto the MOF (SOR-MIL-53). We conclude from the current study that MOF as a carrier is considered a promising nanocarrier for enhancing drug potency as an anti-cancer agent, though selectivity improvements remain modest. Loading Sorafenib on MOF showed enhanced potency on HepG2 cell lines and demonstrated potential for colorectal cancer applications, despite sorafenib not being FDA-approved for this indication.

Keywords Hepatocellular carcinoma (HCC), Chemotherapy, Sorafenib, HepG2, HCT-116, Metal-organic framework (MOF), MTT assay, Sensitivity, And selectivity index, Nanomedicine

[1]Biotechnology Department, Faculty of Science, Cairo University, Giza 12613, Egypt. [2]Faculty of Biotechnology, October University for Modern Sciences and Arts (MSA University, 6 October City, Egypt. [3]Chemistry Department, Faculty of Science, Beni Suef University, Beni Suef 2722165, Egypt. [4]Biology Department, Faculty of Science, King Khalid University, P.O. Box 9004, Abha 61413, Saudi Arabia. [5]Blood Products Quality Control and Research Department, National Organization for Research and Control of Biologicals, Cairo, Egypt. ✉email: elzayatem@sci.cu.edu.eg; nyehia@sci.cu.edu.eg

Cancer is responsible for around one out of every six deaths globally. It is the globe's second-greatest cause of death, with a stated 8.7 million fatalities[1]. Cancer represents a group of diseases or illnesses described by the free limits' development and migration of aberrant cells. If cancer cell propagation, also known as metastasis, remains untreated, this could give rise to dying. The prognosis for liver cancer is poor. Only 5–15% of patients are eligible for surgical removal, which is suitable only for early-stage patients, and due to diminished hepatic regenerative capacity, typically without cirrhosis; right hepatectomy carries a higher risk for post-operative complications compared to left hepatectomy[2]. Colorectal cancer (CRC) is the third most common cause of cancer and the second most common cause of cancer-related death worldwide. Despite increasing survival rates, metastatic CRC (mCRC) remains a lethal disease with a 5-year survival rate of approximately 14%[3].

Chemotherapy, as one of the main traditional therapy methods, has been largely indispensable in cancer treatment[4]. Unfortunately, due to the inevitable adverse effects, drug resistance, and the complexity and heterogeneity of malignancies, chemotherapy alone often cannot achieve a satisfactory therapeutic outcome[5]. Conventional chemotherapy suffers some limitations[6] (a) Limited aqueous solubility: Most chemotherapeutics either from a plant source or synthetic are hydrophobic and require solvents to formulate the dosage form which contributes to severe toxicity[6] (b) Lack of selectivity of anticancer drugs: Most chemotherapeutics lack selectivity toward cancerous cells cause significant damage to rapidly proliferating normal cells[4] and (c) Multidrug resistance (MDR): MDR is mainly due to increased efflux pumps such as P-glycoprotein (Pgp) in the cell membrane which are responsible for transport of various anticancer drugs out of cells[1].

Nanotechnology has sparked a rapidly growing interest as it promises to solve some issues associated with conventional therapeutic agents, including their poor water solubility (at least, for most anticancer drugs), lack of targeting capability, nonspecific distribution, systemic toxicity, and low therapeutic index[7].

Sorafenib (SOR) oral administration of the multi-kinase inhibitor is recommended worldwide as the first-line therapy for advanced stages of HCC[2]. It is the first orally active tyrosine kinase inhibitor (TKI) approved by the Food and Drug Administration (FDA) for hepatocellular carcinoma treatment. Sorafenib mainly targets vascular endothelial growth factor (VEGFR1-3) and Raf kinases[8–10]. Other reported targets include K-Ras, BRAF, V599E mutant BRAF, platelet-derived growth factor receptor-b(PDGFR-b), FMS-like tyrosine kinase 3 (FLT3), c-Kit and RET, and several other receptor tyrosine kinases (RTKs) via various modes of action, such as inhibition of the Ras/Raf/MAPK and PI3K/AKT/mTOR signaling pathways[11]. Sorafenib leads to clinically significant adverse events (AEs) e.g., diarrhea, hypertension, hand-foot skin reaction, and fatigue, for lacking tumor specificity[12].

While sorafenib is not FDA-approved for colorectal cancer treatment, preclinical studies have demonstrated its activity against CRC cell lines through inhibition of VEGFR and Raf kinases, which are also relevant targets in colorectal carcinogenesis[13]. The inclusion of HCT-116 colorectal cancer cells in this study aims to explore the potential of MOF-delivered sorafenib to expand its therapeutic applications beyond its current FDA-approved indication. This approach is supported by research showing that sorafenib can inhibit p38α activity in colorectal cancer cells and synergize with other inhibitors to increase apoptotic response[13]. The enhanced delivery and controlled release provided by MOF encapsulation may overcome some of the limitations that have prevented sorafenib's clinical success in CRC, potentially opening new therapeutic avenues.

Nanotechnology has been considered an applied technology in various areas in recent decades[14,15]. Nanotechnology has been developed by a convergence of various sciences, providing a way to work at the atomic level and to create new structures. Nanotechnology includes the production of nanosized materials and devices and controlling them to use their unique characteristics[16]. Nanotechnology-based drug delivery systems initially include nanoparticles that contain one or more therapeutic drugs that can bind or scatter and adsorbed polymer matrices[14,15]. In the last few years, there has been significant development in nano-drug production using imagery, treatments, and diagnostics. Nano-drug systems primarily focus on improving the bioavailability of specific tissue delivery, extending injectable medicines' half-life, and orally giving medicinal products[17].

Metal-organic frameworks (MOFs) represent a new class of porous materials. They have a modular structure, which offers enormous structural diversity and wide possibilities for the creation of materials with tailored properties[18]. MOFs serve as promising drug nanocarriers owing to their high porosity and large surface area, together with the synthetic tunability that enables the integration of phototherapies, chemodynamic therapy (CDT), ferroptosis therapy, and other therapy strategies[19]. The enhanced permeability and retention (EPR) effect allows MOF nanocarriers to preferentially accumulate in tumor tissues due to their leaky vasculature and poor lymphatic drainage, providing a passive targeting mechanism that can improve drug selectivity[20]. MOF nanocarriers satisfying multifaceted requirements including controlled drug loading and release, therapeutic efficacy, and biocompatibility remain challenging[21]. Besides, high batch-to-batch variation of commonly developed drug-laden MOFs renders them lacking flexibility, precision, and versatility in specific elaborative applications[22]. Therefore, the development of novel multifunctional, stable, and accurate MOF-based delivery systems for efficient multimodal therapy is still highly sought after[23]. The goal of the present study is to test the hypothesis that loading SOR onto MOF as a nanocarrier can improve sorafenib's sensitivity and selectivity against hepatocellular cancer and colorectal cancer cell lines.

Materials & methods

Cell culture

Human hepatocellular carcinoma (HepG2) and human colorectal cancer (HCT-116) cell lines as well as normal human skin cell line (HFb-4) were supplied by Creative Egyptian Biotechnologist Giza, Egypt. The HepG2 cell line was purchased from ATCC, USA, and HFb-4 was purchased from VACSERA Egypt and used in the study. The HepG2 and HCT-116 cells were routinely cultured in DMEM while HFb-4 cells were routinely cultured in RPMI-160. The complete media is supplemented with 10% fetal bovine serum (FBS), 2 mM L-glutamine, containing 100 units/ml penicillin G sodium, 100 units/mL streptomycin sulfate, and 250 ng/mL amphotericin B. All from Lonza, (Basel, Switzerland). Cells were maintained at sub-confluency at 37 °C in humidified air containing 5% CO_2. For sub-culturing, monolayer cells were harvested after trypsin/EDTA treatment at 37 °C. Cells were used when confluence had reached 75%.

Preparation of MIL-53 (Fe)

MIL-53(Fe) (Materials of Institute Lavoisier-53 containing iron) nanoparticles were synthesized using a previously reported hydrothermal method (Gan et al. 2020). Typically, 1.66 g of H2BDC (benzene-1,4-dicarboxylic acid, also known as terephthalic acid) and 2.703 g of $FeCl_3{\cdot}6H_2O$ were dissolved in 50mL dimethylformamide (DMF) with stirring for 10 min. The mixture was transferred to a Teflon-lined stainless steel Parr autoclave (160mL) which was heated in an electric oven at 150 °C for 65 h. The product was filtered, and washed 3 times with DMF, then 3 times with methanol by centrifugation to remove surfactant and unreacted species. The obtained sample was vacuum-dried overnight before characterization. To ensure batch-to-batch reproducibility, multiple batches were synthesized and characterized using PXRD to confirm crystallinity consistency.

Sorafenib (SOR) loading onto MIL-53(Fe) nanoparticles

100 mg of sorafenib aqueous solution was added to an aqueous suspension of 200 mg of MIL-53 and stirred for 48 h at room temperature. The products were then washed 5 times with water by centrifugation (at 10,000 rpm for 20 min) to remove unloaded sorafenib.

Evaluation of hydrodynamic size, polydispersity index (PDI), and zeta potential

To determine the hydrodynamic size and polydispersity index (PDI), the SOR-MIL-53 nanocomposites were analyzed by dynamic light scattering (DLS) using a ZS90 Zetasizer instrument (Malvern, UK). DLS exploits particle motion to obtain size and PDI. The data was examined with Malvern's 'DTS nano' software. A ZS90 Zetasizer (Malvern, UK) was also used to measure the zeta potential of the nanoparticles. All measurements were performed in triplicate. Zeta potential indicates the overall surface charge acquired by particles in a medium, significantly impacting nanoparticle stability. Thus, it is a vital parameter for the characterization.

Fourier transform infrared spectroscopy (FTIR)

Fourier transform infrared spectroscopy (FTIR) was performed to analyze the prepared samples using a Bruker Vertex 70 FTIR-FT Raman spectrometer to determine the compatibility of all components. To prepare the samples, they were mixed with IR-grade potassium bromide and then pressed into discs. The spectra were scanned over an absorption range of 4000– 400 cm^{-1}.

X-ray diffraction (XRD)

Powder X-ray diffraction (PXRD) analysis was performed to evaluate the crystalline structures of prepared powder samples of MIL-53, SOR drug, and SOR-MIL-53 nanocomposites. The samples were analyzed using Cu Kα radiation (λ = 1.54 Å), scanning the powdered materials over a 2θ range of 5 – 70° at a voltage of 40 kV and current of 30 mA. A 2θ/θ scanning range was selected with a scanning speed of 2°/min. Crystallite sizes were calculated using the Scherrer equation: $D = K\lambda/(\beta\cos\theta)$, where D is the crystallite size, K is the shape factor (0.9), λ is the X-ray wavelength, β is the full width at half maximum (FWHM) of the diffraction peak, and θ is the Bragg angle.

Surface area, pore volume, and pore size (BET)

The specific surface areas of nanocomposites were determined using the Brunauer–Emmett–Teller (BET) method. Theory using N_2 adsorption-desorption isotherm (Quantachrome TouchWin Software version 1.21) at 77 K after degassing at 150 °C under vacuum for 3 h. The pore volume and pore size distribution were calculated according to the Barrett–Joyner–Halenda theory (BJH).

Sorafenib (SOR) entrapment efficiency (EE) and loading capacity (LC)

Key metrics for evaluating nanocarrier performance were encapsulation efficiency (EE) and loading capacity (LC) of the bioactive compounds. A 10mL supernatant obtained after centrifugation of SOR-loaded MIL-53 was collected to determine drug loading (DL%) and encapsulation efficiency (EE%) using a UV-vis spectrophotometer measuring absorbance at 265 nm.

The EE% and LC% were calculated using the following equations, which have been cross-verified with established literature[23,24]:

$$\mathrm{EE\%} = (\text{sorafenib content loaded in MIL} - 53\ (\mathrm{Fe})) \ / \ (\text{initial sorafenib content}) \ \text{x}\ 100\%$$

$$\mathrm{DL\%} = (\text{sorafenib content loaded in MIL} - 53\,(\mathrm{Fe})) \ / \ (\text{sorafenib loaded} + \text{weight of MIL} - 53\ (\mathrm{Fe})) \times 100\%$$

In vitro release of SOR from SOR-MIL-53 nanocomposites

The in vitro release profile of SOR from SOR-MIL-53 nanocomposites was compared to free SOR through evaluation in phosphate-buffered saline (PBS, pH 7.4). Sink conditions were maintained throughout the study

by ensuring that the drug concentration remained below 10% of its saturation solubility in the release medium, considering sorafenib's limited aqueous solubility of approximately 0.0068 mg/mL. A dialysis bag (MWCO 12,000–14,000 Da) containing 5mL of free SOR and the equivalent amount of SOR-MIL-53 nanocomposite suspension were incubated in 100mL PBS release medium at 37 °C ± 0.5 °C with a shaking incubator (150 rpm). At the pre-determined time points (0.5, 1, 2, 3, 4, 5, 6, 8, 12, 24, and 48 h), 1 mL aliquots of the samples were collected. After removing, an equal volume of fresh PBS was replaced. The SOR content in the collected samples was quantified by UV-vis spectrophotometry at 265 nm.

Thermal stability

The thermal stability of MIL-53 MOFs and the SOR-MIL-53 nanocomposites was investigated by thermogravimetric analysis using Perkin-Elmer Pyris (TGA) (Massachusetts, USA) and a heating rate of 10 °C per min ranging from 50 to 600 °C under a nitrogen atmosphere.

In vitro cytotoxicity (MTT assay)

The MTT (3-[4, 5-dimethylthiazole-2-yl]-2, 5-diphenyltetrazolium bromide) (Merck KGaA (Darmstadt, Germany), was used to assess the cytotoxicity of the tested samples. Briefly, Cells (1×10^4 cells/well) were seeded in serum-free media in a flat bottom 96-well microplate and treated with 20µL of different concentrations ranging from 50 to 1.5625 µg/mL of the tested samples for 48 h at 37 °C, in a humidified 5% CO_2 atmosphere. After incubation, media was removed and 40µL MTT solution /well was added and incubated for an additional 4 hours. MTT crystals were solubilized by adding 180µL of acidified isopropanol/well and the plates were shacked at room temperature, followed by photometric determination of the absorbance at 570 nm using microplate ELISA reader (FLUOstar OPTIMA, BMG LABTECH GmbH, Ortenberg, Germany). All experiments were performed in triplicate ($n = 3$) with three independent biological replicates. Three times repeats were performed for each concentration and the average was calculated.

Apoptosis and cell cycle progression analysis using flow cytometry

The percentage of HepG2 cells undergoing apoptosis was assessed using flow cytometry with the Annexin V-FITC Apoptosis Detection Kit (BioVision, CA, USA). Additionally, cell cycle analysis was conducted via DNA content staining with propidium iodide (PI) using flow cytometry. Following 24 h of treatment, up to 1×10^5 cells were trypsinized and washed in serum-containing media. The cell suspension was centrifuged at 300×g for 10 min, the supernatant was removed, and the pellet was resuspended in 500 µl of 1X binding buffer. Subsequently, the cells were incubated with 5 µl of Annexin V-FITC and 5 µl of propidium iodide for 5 minutes in the dark. Quantification was performed using a BD FACS Calibur flow cytometer (BD Bioscience, CA, USA).

Statistical analysis

The experimental data was statistically analyzed by student-independent T-test using GraphPad Prism version 10.2.1. For multi-group comparisons involving MOF vs. SOR vs. SOR-MIL-53, ANOVA with post-hoc tests would be more appropriate and is recommended for future studies. Data were accepted as significantly different when $p < 0.05$. All experiments were performed with $n \geq 3$ biological replicates.

Results

The entrapment efficiency (EE) and loading capacity (LC) of SOR-MIL-53 nanocomposite

As illustrated in Table 1, the SOR-MIL-53 formulation achieved a high entrapment efficiency (EE) of 88.97% ± 3.2%, indicating that a significant portion of sorafenib was successfully encapsulated within MOF. This high EE suggests that the MOF is highly effective in incorporating sorafenib, which is essential for ensuring the drug's sustained release and targeted delivery. On the other hand, the loading capacity (LC) of 23.5% ± 11% reflects the amount of sorafenib relative to the total weight of the sorafenib/MOF complex. The relatively high variability in LC (± 11%) indicates potential batch-to-batch reproducibility challenges that require optimization through standardized synthesis protocols and quality control measures. Although the LC is relatively lower and has a wider variation, it is still within an acceptable range for drug delivery systems, showing that the MOF can accommodate a meaningful amount of sorafenib while maintaining its structural integrity.

The in vitro release of SOR-MIL-53 nanocomposite

The in vitro release profile of sorafenib (SOR) from the SOR-MIL-53 nanocomposite, as presented in Table 2; Fig. 1, highlights significant differences in the release behavior between free sorafenib and sorafenib loaded onto the MOF. The free sorafenib exhibited a rapid, short-term release, reaching 100% release within just 5 h. This burst release is typical for free drugs and can potentially limit therapeutic efficacy due to the rapid depletion of the drug from the system. In contrast, the SOR-MIL-53 demonstrated a more controlled, sustained release over 48 h. At the 5-hour, only 69.83% of the drug had been released from the nanocomposite, indicating a slower and more gradual release. This prolonged release is beneficial for maintaining therapeutic drug levels over an extended period, reducing the need for frequent dosing and potentially minimizing side effects associated with drug bursts. Interestingly, the release from SOR-MIL-53 showed steady progress, reaching 74.29% after 12 h and

Entrapment efficiency (EE)	88.97%±3.2%
Loading capacity (LC)	23.5%±11%

Table 1. Entrapment efficiency (EE) and loading capacity (LC) of SOR-MIL-53.

Time (h)	SOR only Release %	SOR-MIL-53 Release %
0	0 ± 0	0 ± 0
0.5	14.2 ± 2.4	17.85 ± 2.1
1	28.24 ± 3.1	32.17 ± 3.2
2	52.32 ± 3.5	51.27 ± 1.9
3	69.24 ± 3.23	59.42 ± 1.6
4	84.35 ± 2.2	66.49 ± 1.2
5	100	69.83 ± 1.1
6		69.99 ± 1
8		71.49 ± 1.1
10		72.93 ± 1.5
12		74.29 ± 1.7
24		83.34 ± 1.9
48		100% ± 12.7

Table 2. Release of free SOR and SOR-MIL-53 over 48 h.

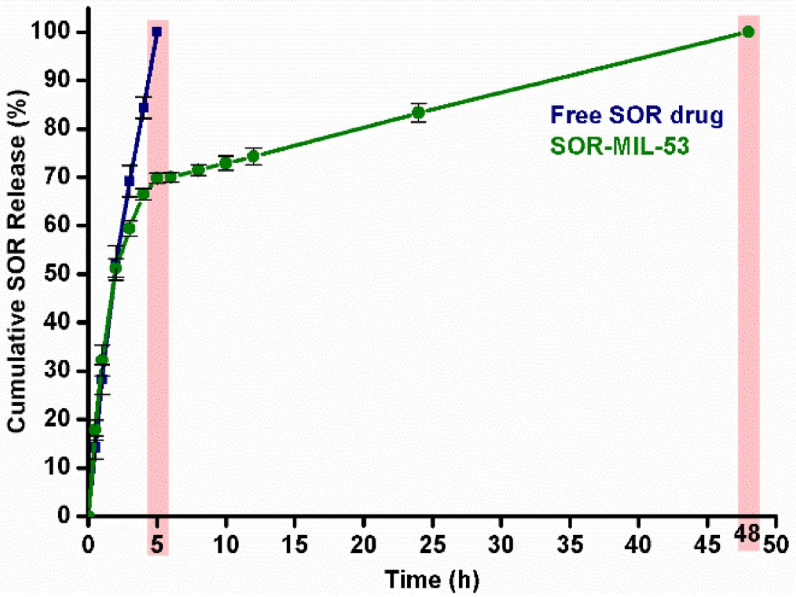

Fig. 1. In vitro release profile over 48 h of free SOR and SOR-MIL-53.

continuing to release until it reached 83.34% at 24 h, to reach its maximum after 48 h. These results demonstrate the potential advantage of using the SOR-MIL-53 nanocomposite over free sorafenib.

Characterization of SOR-MIL-53 nanocomposite

The characterization of MOF/SOR pre- and post-loading via XRD, and FTIR is presented in Fig. 2. The X-ray diffraction (XRD) analysis, as shown in Fig. 2A, reveals critical information about the crystalline structure and drug encapsulation efficiency within the metal-organic framework. The pristine MIL-53 sample, represented by the red trace, exhibits characteristic sharp and well-defined diffraction peaks at approximately 9°, 12°, 18°, and 25° (2θ), which are consistent with the reported crystal structure of MIL-53(Fe). The peak at around 9° corresponds to the (100) reflection, while the peak at 18° represents the (110) reflection, both of which are diagnostic features of the MIL-53 breathing framework structure. The high intensity and sharpness of these peaks confirm the successful synthesis of a highly crystalline MOF with excellent structural integrity. In contrast, the free sorafenib drug, shown in blue, displays a complex diffraction pattern characterized by multiple sharp peaks distributed across the 10–30° (2θ) range. Notable peaks appear at approximately 11°, 15°, 17°, 20°, 22°, and 26° (2θ), indicating that the drug exists in a highly crystalline state with a well-defined polymorphic form. The multiplicity and sharpness of these peaks reflect the complex molecular structure of sorafenib and its tendency to form stable crystalline arrangements. The most significant findings emerge from the analysis of the SOR-MIL-53 composite, represented by the green trace. While the characteristic peaks of the MIL-53 framework are largely preserved, indicating that the MOF structure remains intact after drug loading, there is a remarkable reduction or complete disappearance of the characteristic sorafenib diffraction peaks. This observation provides

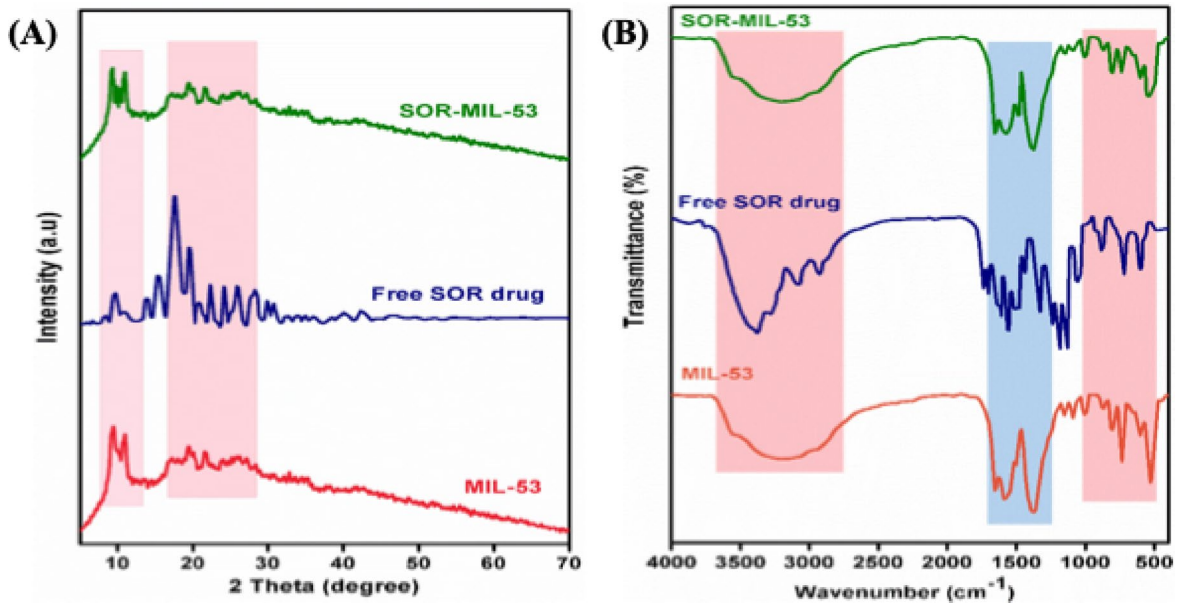

Fig. 2. Characterization of MOF/SOR pre- and post-loading. (**A**) XRD, and (**B**) FTIR of MIL-53, free SOR, and SOR-MIL-53 nanocomposites.

compelling evidence for successful drug encapsulation within the MOF pores. The absence of sharp sorafenib peaks suggests that the drug has transitioned from its crystalline state to an amorphous or molecularly dispersed form within the framework cavities. This amorphization is particularly advantageous for pharmaceutical applications, as amorphous drugs typically exhibit enhanced solubility and dissolution rates compared to their crystalline counterparts. Additionally, some broadening of the MOF peaks in the composite may indicate slight structural strain or size effects resulting from drug incorporation, though the overall framework integrity is maintained.

Additionally, the FTIR analysis, as shown in Fig. 2B, provides detailed molecular-level information about the functional groups present in each sample and the nature of drug-framework interactions. Examining the high-frequency region between 3000 and 4000 cm^{-1}, the pristine MIL-53 spectrum shows a broad absorption band around 3300–3500 cm^{-1}, which is characteristic of O-H stretching vibrations from coordinated water molecules or hydroxyl groups associated with the iron metal centers. The free sorafenib spectrum exhibits distinct sharp peaks at approximately 3332 and 3296 cm^{-1}, corresponding to N-H stretching vibrations from the drug's amine functional groups. In the SOR-MIL-53 composite, these N-H peaks become broadened and slightly shifted, indicating the formation of hydrogen bonding interactions between the drug molecules and the MOF framework. The mid-frequency region spanning 1400–1800 cm^{-1} reveals important information about the carboxyl and carbonyl functionalities. The MIL-53 spectrum displays characteristic peaks at approximately 1680 cm^{-1}, attributed to C = O stretching of carboxyl groups, and at 1579 cm^{-1}, corresponding to the symmetric stretching of COO^- groups from the benzene-1,4-dicarboxylic acid (BDC) linkers coordinated to the iron centers. The free sorafenib spectrum shows a prominent peak at around 1740 cm^{-1}, representing amide C = O stretching, along with multiple peaks in the 1400–1600 cm^{-1} region that correspond to aromatic C = C and C = N stretching vibrations. The composite spectrum exhibits overlapping features from both components, with slight shifts in peak positions that further confirm drug-MOF interactions while preserving the essential functional groups of both materials. The fingerprint region below 1400 cm^{-1} provides additional confirmation of successful composite formation. The MIL-53 spectrum shows a characteristic peak at approximately 535 cm^{-1}, which is diagnostic of Fe-O stretching vibrations and confirms the metal-ligand coordination within the framework. This peak is preserved in the composite spectrum, indicating that the MOF structure remains intact after drug loading. The free sorafenib spectrum exhibits peaks at 1296 and 1126 cm^{-1}, corresponding to C-O stretching vibrations from carboxylic acid groups, along with a complex fingerprint pattern characteristic of the drug's molecular structure. The composite spectrum shows a combination of features from both components, with some peak shifts and intensity modifications that reflect the changed molecular environment upon drug encapsulation.

The combined XRD and FTIR analysis provides compelling evidence for the nature of drug-framework interactions within the SOR-MIL-53 composite. The spectroscopic data suggests that sorafenib encapsulation occurs primarily through physical interactions rather than chemical bonding. The slight shifts and broadening observed in the FTIR peaks indicate the presence of weak intermolecular forces, including hydrogen bonding between the drug's amine groups and the framework's oxygen atoms, potential π-π stacking interactions between aromatic rings, and van der Waals forces within the confined pore environment. The absence of new peaks in either the XRD or FTIR spectra confirms that no covalent bonds are formed between the drug and the MOF, which is advantageous for maintaining drug bioactivity and enabling controlled release. The transition of sorafenib from a crystalline to an amorphous state upon encapsulation has significant implications for drug

delivery applications. Amorphous drugs typically exhibit higher apparent solubility and faster dissolution rates compared to their crystalline forms, which can lead to improved bioavailability. The molecular dispersion of sorafenib within the MOF pores, as evidenced by the complete suppression of drug crystalline peaks in the XRD pattern, suggests efficient utilization of the available pore space and high loading efficiency. Furthermore, the preservation of the MOF's structural integrity, as confirmed by the retention of characteristic diffraction peaks and vibrational bands, ensures that the framework can provide the necessary mechanical stability and controlled release properties. The characterization results have important implications for the performance of the SOR-MIL-53 system as a drug delivery vehicle. The amorphous state of the encapsulated drug should facilitate rapid dissolution upon contact with biological fluids, potentially leading to faster onset of therapeutic action. The physical nature of the drug-framework interactions suggests that drug release will be governed by diffusion processes rather than chemical dissociation, enabling fine-tuning of release kinetics through control of particle size, pore structure, and environmental conditions. The maintained structural integrity of the MOF framework ensures that the system can withstand physiological conditions while providing protection for the encapsulated drug against degradation. The absence of unwanted phase formation or chemical degradation, as confirmed by the clean spectroscopic profiles, indicates excellent compatibility between sorafenib and the MIL-53(Fe) framework. This compatibility is crucial for maintaining drug stability during storage and ensuring predictable release behavior in biological environments. The successful encapsulation without compromising the functional groups of either component suggests that the therapeutic efficacy of sorafenib should be preserved while benefiting from the enhanced delivery properties provided by the MOF carrier.

Hydrodynamic size, PDI, and zeta potential of SOR-MIL-53 nanocomposite

The characterization data presented provides crucial insights into the surface properties and particle size distribution of the MIL-53(Fe) metal-organic framework before and after sorafenib loading. The analysis encompasses zeta potential measurements and dynamic light scattering (DLS) particle size distribution, which are fundamental parameters for understanding the colloidal stability and physical properties of the nanocomposite system (Fig. 3). The zeta potential measurements reveal significant differences between the pristine MIL-53 framework and the sorafenib-loaded composite (Fig. 3A). The pristine MIL-53 exhibits a zeta potential of approximately 29.0 ± 2.0 mV, indicating a strong positive surface charge. This positive charge can be attributed to the iron(III) metal centers within the framework structure, which contribute to the overall electrostatic properties of the MOF surface. The relatively high absolute value of the zeta potential suggests excellent colloidal stability, as particles with zeta potential values above ± 25 mV typically demonstrate good resistance to aggregation due to strong electrostatic repulsion between particles. Following sorafenib encapsulation, the SOR-MIL-53 composite shows a notably reduced zeta potential of approximately 13.0 ± 2.5 mV. This significant decrease in surface charge can be attributed to several factors related to drug loading. The encapsulation of sorafenib molecules within the MOF pores may partially shield the positive charges of the iron centers, leading to a reduction in the overall surface charge density. Additionally, sorafenib molecules may interact with the framework surface through hydrogen bonding or electrostatic interactions, further modifying the surface charge distribution. The drug molecules themselves may contribute neutral or slightly negative charges that counterbalance the positive framework charges. Despite the reduction in zeta potential magnitude, the SOR-MIL-53 composite maintains a positive surface charge, which is beneficial for several reasons. The positive charge can enhance cellular uptake through electrostatic interactions with negatively charged cell membranes, potentially improving the therapeutic efficacy of the drug delivery system. However, the reduced absolute value suggests that additional stabilization mechanisms, such as steric stabilization or the use of surfactants, might be beneficial for long-term colloidal stability, particularly in high ionic strength environments.

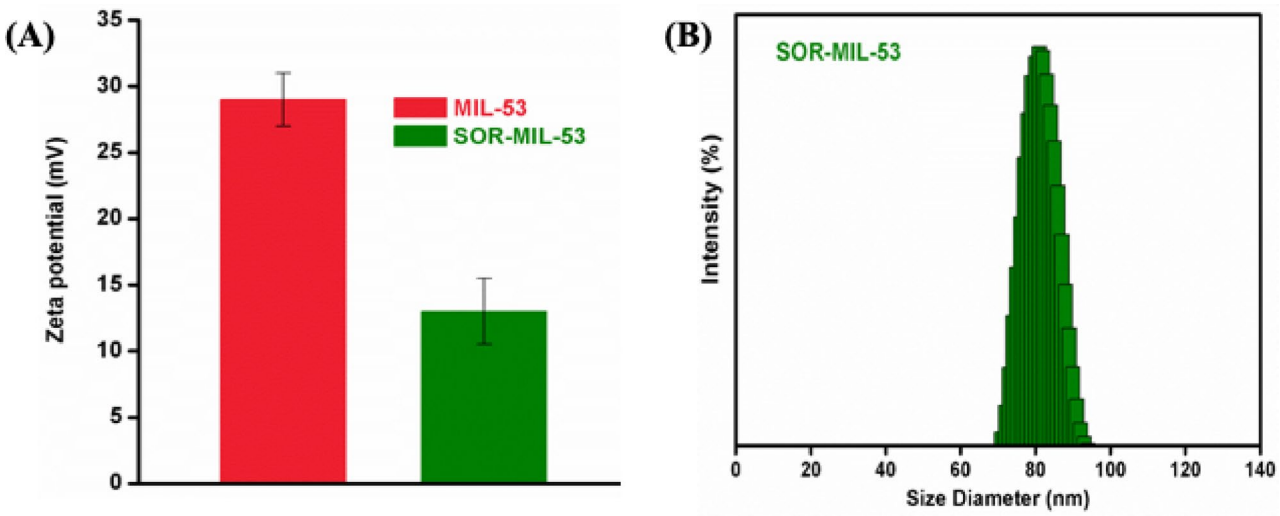

Fig. 3. (**A**) Zeta potential of MIL-53, and SOR-MIL-53 nanocomposites, and (**B**) Particle size analysis of SOR-MIL-53 nanocomposites.

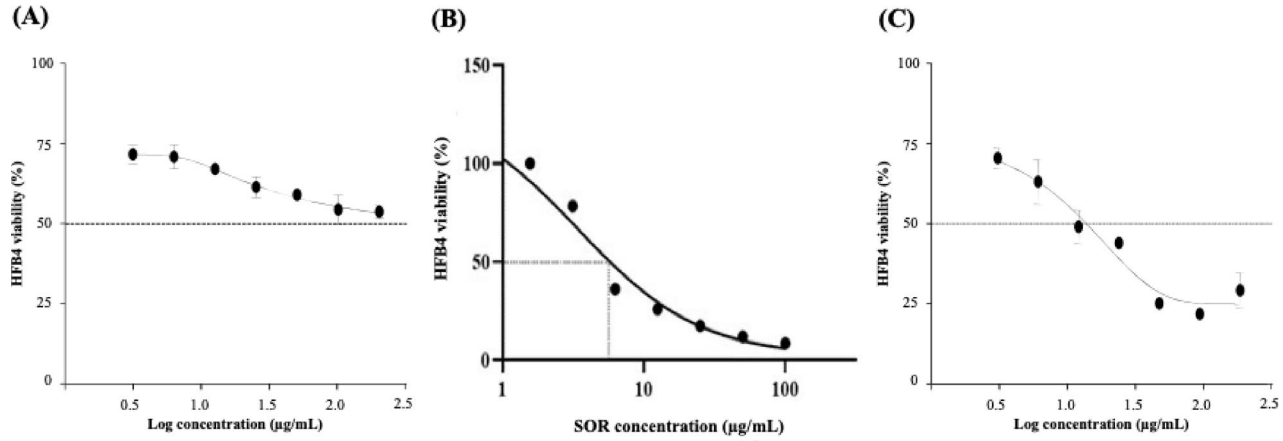

Fig. 4. A dose-response sigmoid curve in a logarithmic concentration of human fibroblast cell line (HFb-4) 48 h post-treatment with (**A**) MOF, (**B**) SOR, and (**C**) SOR-MIL-53 nanocomposites.

Cell line	IC_{50} SOR	SI	IC_{50} SOR-MIL-53 before correction	IC_{50} SOR-MIL-53 after correction	SI
HFb-4	5.88 µg/ml	-	14.22 µg/ml	3.3 µg/ml	-
HepG2	12.58 µg/ml	0.46	23.49 µg/ml	5.5 µg/ml	0.6
HCT-116	12.73 µg/ml	0.2	33.72 µg/ml	7.9 µg/ml	0.42

Table 3. The selectivity index (SI) and IC_{50} of MOF and SOR before and after loading on HFb-4, HepG2, and HCT-116 cell lines.

The dynamic light scattering analysis of the SOR-MIL-53 composite reveals a narrow and well-defined particle size distribution, which is crucial for consistent drug delivery performance (Fig. 3B). The distribution shows a single, sharp peak centered at approximately 80 nm, with the majority of particles falling within the 70–95 nm range. This narrow size distribution indicates excellent batch-to-batch reproducibility and uniform particle formation during the synthesis and drug loading processes. The mean particle size of 80 nm is particularly advantageous for biomedical applications. Particles in this size range are optimal for several reasons: they are small enough to avoid rapid clearance by the reticuloendothelial system, yet large enough to carry substantial drug payloads. This size range also facilitates enhanced permeability and retention (EPR) effect in tumor tissues, where the leaky vasculature allows preferential accumulation of nanoparticles while normal tissues with tight endothelial junctions exclude them. The size is also suitable for cellular uptake through endocytosis mechanisms, ensuring efficient intracellular drug delivery. The symmetrical nature of the distribution curve suggests that the particles are relatively monodisperse, with minimal presence of aggregates or secondary particle populations. This uniformity is essential for predictable pharmacokinetic behavior and consistent therapeutic outcomes. The absence of a significant tail in the distribution indicates that the synthesis and drug loading processes do not induce substantial particle aggregation, which could otherwise lead to variable drug release kinetics and potential safety concerns related to embolism.

The combination of zeta potential and particle size data provides valuable insights into the expected performance of the SOR-MIL-53 system in biological environments. The positive surface charge, while reduced compared to the pristine MOF, should facilitate interactions with negatively charged biological membranes and potentially enhance cellular uptake. The moderate zeta potential value suggests that the particles will maintain reasonable stability in physiological conditions while avoiding excessive electrostatic interactions that could lead to non-specific binding or toxicity. The narrow particle size distribution centered around 80 nm positions the SOR-MIL-53 composite in an optimal size range for passive tumor targeting through the EPR effect. This size allows the particles to extravasate through the fenestrated tumor vasculature while being retained due to poor lymphatic drainage. Simultaneously, the particles are small enough to penetrate deep into tumor tissue and reach cancer cells that are distant from blood vessels.

The cytotoxicity and selectivity index (SI) before and after loading Sorafenib on MOF on different cell lines

The cytotoxicity of the MOF, SOR, and SOR-loaded MOF nanocomposites was evaluated on normal human fibroblast cells (HFb-4), as presented in Fig. 4; Table 3. The results showed a typical sigmoid dose-response curve when plotting the concentration of the compounds against cell viability using GraphPad Prism software. The half-maximal inhibitory concentration (IC_{50}) values for MOF, SOR, and SOR/MOF were determined as > 200 µg/mL, 5.88 µg/mL, and 14.22 µg/mL, respectively, before correction for loading capacity. After adjusting for loading capacity, the IC_{50} value for the SOR/MOF nanocomposite was calculated to be 3.3 µg/mL. These findings suggest

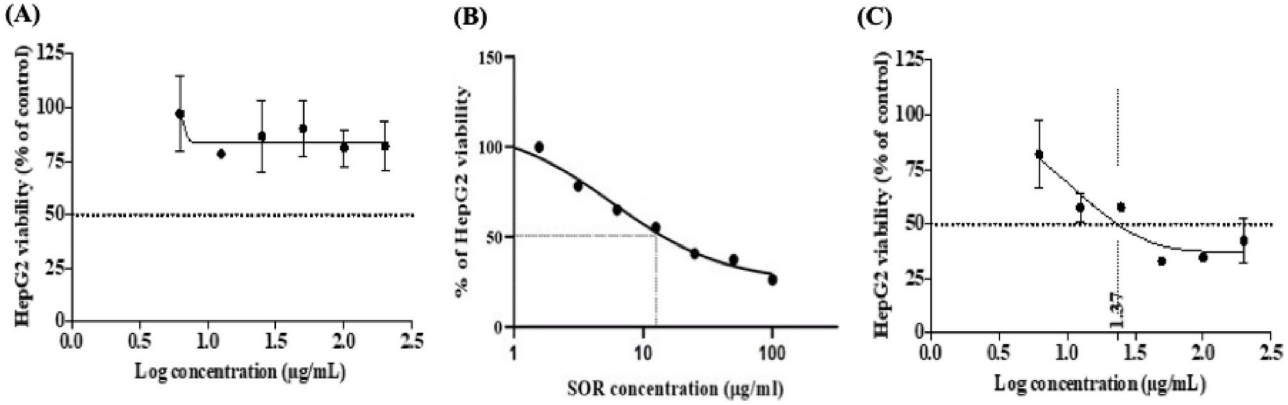

Fig. 5. A dose-response sigmoid curve in a logarithmic concentration of hepatoblastoma cell line (HepG2) 48 h post-treatment with (**A**) MOF, (**B**) SOR, and (**C**) SOR-MIL-53 nanocomposites.

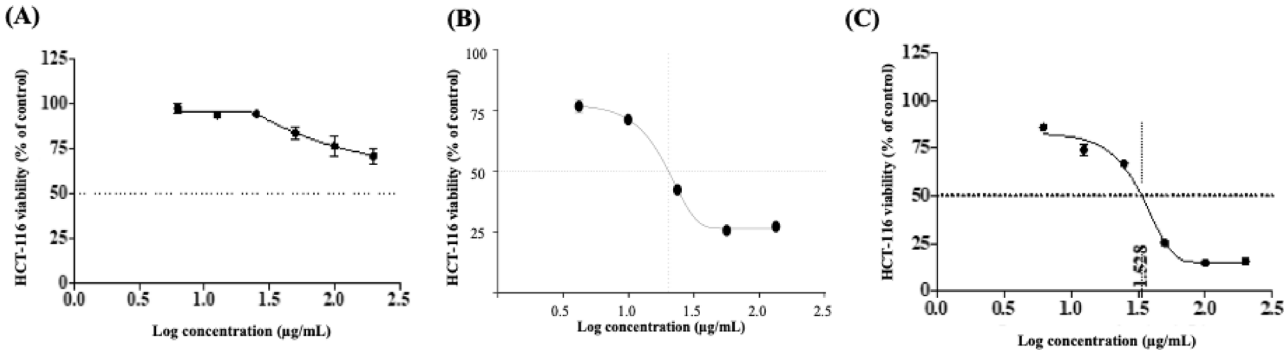

Fig. 6. A dose-response sigmoid curve in a logarithmic concentration of human colorectal carcinoma cell line (HCT-116) 48 h post-treatment with (**A**) MOF, (**B**) SOR, and (**C**) SOR-MIL-53 nanocomposites.

that while the MOF alone is relatively non-toxic to normal cells, the SOR-MIL-53 nanocomposite shows a moderate level of cytotoxicity, demonstrating enhanced potency compared to free SOR, implying a controlled and less harmful release mechanism.

Figure 5; Table 3 presents the cytotoxicity results on HepG2 hepatocellular carcinoma cells, showing a clear dose-response relationship. The IC_{50} values obtained for MOF, SOR, and SOR-MIL-53 were >200 µg/mL, 12.58 µg/mL, and 23.49 µg/mL, respectively, before correction. After adjusting for loading capacity, the IC50 of the SOR-MIL-53 nanocomposite dropped to 5.5 µg/mL. This indicates that the SOR-MIL-53 nanocomposite exhibits potent cytotoxicity against HepG2 cells, with enhanced potency post-loading capacity correction compared to the free drug. The significantly lower IC50 after adjustment reflects the enhanced therapeutic effect and suggests a more efficient drug release mechanism from the MOF nanocomposite.

The cytotoxic effect of MOF, SOR, and SOR-MIL-53 was further assessed on human colorectal carcinoma cells (HCT-116), as illustrated in Fig. 6; Table 3. The IC_{50} values were determined as >200 µg/mL for MOF, >200 µg/mL for SOR, and 33.72 µg/mL for the SOR-MIL-53 nanocomposite before correction. After loading capacity correction, the IC50 of the SOR-MIL-53 nanocomposite decreased to 7.9 µg/mL. This indicates that the SOR/MOF nanocomposite exerts a much stronger cytotoxic effect on HCT-116 cells compared to the free drug, especially after loading adjustment, making it a potentially more effective treatment option for colorectal cancer.

The selectivity index (SI) was calculated using the formula: SI = IC_{50} (normal cells) / IC_{50} (cancer cells). For HepG2 cells, the SI improved from 0.46 (free SOR) to 0.6 (SOR-MIL-53), representing a 30% improvement. For HCT-116 cells, the SI increased from 0.2 to 0.42, showing a 110% improvement. However, it is important to note that all SI values remain below 1, and ideally, a clinically relevant selectivity index should be >2. These improvements indicate that further optimization is needed to achieve clinically meaningful selectivity. The modest SI values suggest that the current formulation enhances potency more effectively than selectivity, and future research should focus on active targeting strategies to improve cancer cell specificity.

Overall, these results indicate that loading sorafenib onto MOF enhances its cytotoxic efficacy, making it more potent across cancer cell lines. However, the selectivity improvements remain modest and require further investigation to ensure that the enhanced efficacy translates to clinically relevant therapeutic windows.

	Untreated control	SOR/MOF	*P*-value
Viable cells	95.89% ± 11.25	18.49% ± 2.15*↓	0.0002
Necrosis	2.71% ± 0.17	36.79% ± 3.67*↑	0.0001
Late Apoptosis	0.13% ± 0.009	38.31% ± 2.5*↑	0.00001
Early Apoptosis	1.27% ± 0.011	6.41% ± 0.67*↑	0.0002

Table 4. Apoptotic and necrotic effects of IC_{50} of SOR-MIL-53 nanocomposite as analyzed by flow cytometry in the HepG2 cancer cell line after 24-hour treatment.

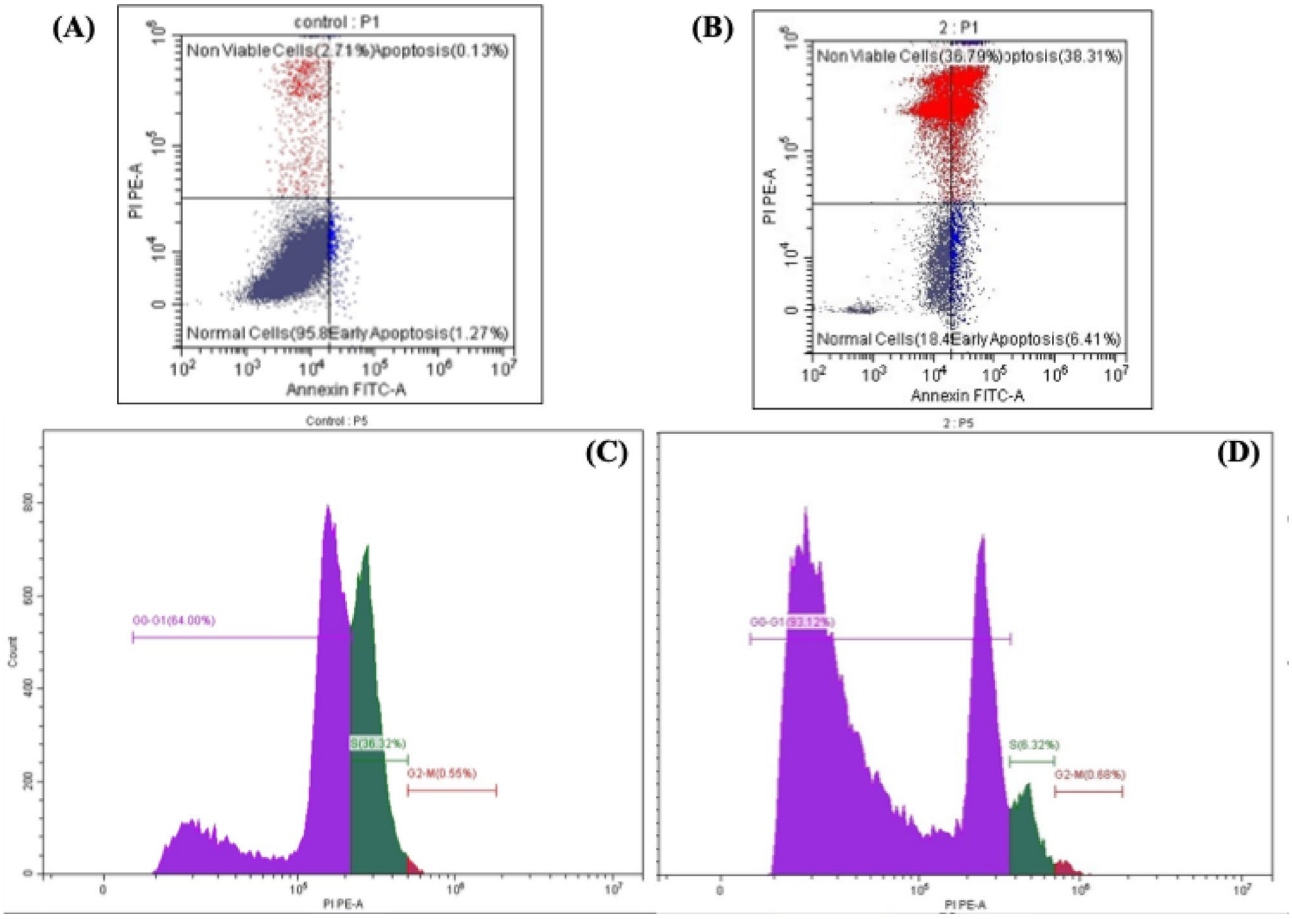

Fig. 7. Schematic representation of the apoptotic activity and cell cycle profile of nanocomposite IC_{50} after treatment for 24 h on the HepG2 cancer cell line. (**A** and **B**) Apoptosis activity; (**A**) Annexin V/PI (untreated control); (**B**) Annexin V/PI (treated with 23.49 µg/ml SOR-MIL-53). The right lower quadrant represents annexin V positive/PI negative staining, indicating early apoptosis. The right upper quadrant represents both high annexin V and PI staining, indicating late apoptosis, and the left upper quadrant represents low annexin V and high PI staining, indicating necrosis. (**C** and **D**) Cell cycle profile; (**C**) cell count in the cell cycle stages (untreated control), (**D**) cell count in the cell cycle stages (treated with 23.49 µg/ml SOR-MIL-53).

Analysis of apoptosis, necrosis, and cell cycle profile using flow cytometry

The apoptotic and necrotic effects of SOR-MIL-53 nanocomposites at their IC_{50} concentrations were evaluated using flow cytometry across the HepG2 cell line after 24 h of treatment. The results, summarized in Table 4; Fig. 7 **(A & B)**, reveal a significant increase in early apoptosis, late apoptosis, and necrotic cell percentages in response to SOR-MIL-53 treatment ($p < 0.05$). These findings align with the cytotoxicity results, confirming that SOR-MIL-53 effectively induces apoptosis in HepG2 cancer cell lines.

The impact of SOR-MIL-53 at its IC_{50} concentration on the cell cycle distribution of cancer cell lines was also assessed. As shown in Table 5; Fig. 7 **(C & D)**, a significant increase ($p < 0.05$) in the proportion of cells in the G0-G1 was observed, along with a marked decrease in the S phase. These changes indicate cell cycle arrest at the G0-G1 phase due to SOR-MIL-53 treatment, with HepG2 cells exhibiting the most pronounced effects.

Nanocomposite	Treatment	%G0-G1	%S	%G2-M
SOR-MIL-53	Untreated HepG2 Control	64.00 ± 4.03	36.32 ± 1.23	0.55 ± 0.17
	IC_{50} (23.49 µg/ml)	93.12 ± 2.16*↑	6.32 ± 2.34*↓	0.68 ± 0.95
	***P*-value**	0.0004	0.00004	0.83

Table 5. Effect of SOR-MIL-53 nanocomposite on the different phases of the cell cycle as analyzed by flow cytometry in HepG2 cell line after 24 h treatment.

Discussion

Cancer is a leading global health challenge, responsible for approximately one in six deaths worldwide[25]. Hepatocellular carcinoma and colorectal cancer are among the most prevalent and lethal forms of cancer, with HCC being the second leading cause of cancer-related deaths and CRC the third most common cancer globally[26]. Current treatment strategies, including chemotherapy, targeted therapies, and surgery, often suffer from limitations such as systemic toxicity, poor drug selectivity, and multiple drug resistance (MDR), which decrease their effectiveness and lead to adverse side effects[4,5,27,28].

Sorafenib (SOR), a multikinase inhibitor, has been widely used in the treatment of HCC and CRC due to its ability to inhibit key molecular pathways involved in tumor progression[13,29–31]. Specifically, SOR targets serine/threonine kinases in the Ras-Raf-MEK-ERK signaling pathway, which is crucial for tumor angiogenesis and growth[11,32]. It also inhibits VEGFR and PDGFR, leading to the suppression of blood vessel formation that supports tumor growth[33,34]. However, despite its therapeutic potential, SOR has limitations, including poor aqueous solubility and off-target toxicity, so searching for better delivery mechanisms is essential[35].

Metal-organic frameworks (MOFs), particularly MIL-53(Fe), have gained attention as drug delivery systems due to their unique structural properties[19]. MOFs offer large surface areas, high porosity, and the ability to encapsulate drugs with high loading efficiency[19,21]. Moreover, MOFs' controlled release mechanisms can enhance the targeting of cancer cells while minimizing damage to normal tissues[36,37]. The enhanced permeability and retention (EPR) effect allows MOF nanocarriers to preferentially accumulate in tumor tissues due to their leaky vasculature and poor lymphatic drainage, providing a passive targeting mechanism that can improve drug selectivity[20]. MIL-53(Fe) stands out for its biocompatibility, large pore size, and capacity for drug loading[38,39]making it an excellent candidate for delivering hydrophobic drugs like sorafenib. By loading SOR onto MOFs, it is possible to improve its solubility, stability, and potency, thus potentially overcoming the limitations of traditional chemotherapy.

In this study, we explored the effectiveness of sorafenib-loaded MOFs (SOR-MIL-53) in enhancing anticancer activity against hepatocellular carcinoma (HepG2) and colorectal cancer (HCT-116) cell lines, while reducing toxicity to normal cells (HFb-4). This approach aims to open the way to improving drug targeting and therapeutic outcomes, addressing critical challenges in cancer treatment by combining sorafenib with advanced nanotechnology-based delivery systems. By incorporating SOR into the MOF structure, we observed a significant increase in the drug's potency and modest improvements in selectivity, with higher cytotoxic effects against cancer cells compared to normal cells.

The loading of sorafenib onto MIL-53 (Fe) resulted in an impressive entrapment efficiency of 88.97% ± 3.2% and a loading capacity (LC) of 23.5% ± 11%. The high variability in LC (± 11%) represents a significant challenge for batch-to-batch reproducibility and indicates the need for optimized synthesis protocols and stringent quality control measures. These values suggest a robust drug delivery system, consistent with findings from Li et al. (2022), who achieved similar results when loading chemotherapeutic agents such as doxorubicin onto MOFs[24]. The spontaneous release of SOR from the MOF structure after 48 h further confirmed the MOF's capability as an efficient carrier system, allowing for sustained drug release, which is crucial for therapeutic efficacy. However, future studies should investigate release profiles under acidic conditions (pH 5.0-6.5) to validate tumor-specific release mechanisms and confirm the potential for pH-responsive drug delivery.

Notably, the IC_{50} values for SOR-MIL-53 decreased significantly across all tested cell lines. In HepG2 cells, the corrected IC_{50} of 5.5 µg/ml indicated improved drug potency compared to free SOR (IC_{50} of 12.58 µg/ml). Similarly, HCT-116 cells showed enhanced sensitivity, with a corrected IC_{50} of 7.9 µg/ml. These improvements align with previous studies emphasizing the role of MOFs in improving the efficacy of chemotherapeutic agents through enhanced permeability and retention (EPR) effects, as first described by Maeda et al. in 1986 [20]. The reduction in IC_{50} also reflects the ability of MOFs to provide a more targeted drug delivery, thereby minimizing off-target effects on normal cells.

However, while the selectivity index (SI) showed modest improvements in HepG2 and HCT-116 cells (SI of 0.6 and 0.42, respectively), these values remain below the clinically relevant threshold of > 2. This limitation indicates that the current MOF formulation enhances potency more effectively than selectivity. The relatively low SI values suggest the need for further optimization strategies, including surface modification for active targeting, incorporation of targeting ligands, or development of stimuli-responsive release mechanisms to achieve clinically meaningful selectivity toward cancer cells over normal cells[40,41]. The ability of MOFs to protect and slowly release SOR offers a promising approach to overcoming the limitations of traditional chemotherapy, such as low aqueous solubility and multiple drug resistance (MDR)[6,41].

The observed increase in early and late apoptosis, as well as necrotic cell percentages following SOR-MIL-53 treatment, highlights the potential of this nanocomposite as a potent inducer of programmed cell death in cancer cells[29,36]. This is consistent with its cytotoxic effects observed in prior assays, suggesting that SOR-MIL-53 disrupts cellular homeostasis, leading to apoptotic and necrotic pathways[9,13,19]. The induction of apoptosis might

be attributed to sorafenib's interaction with key apoptotic regulators, such as caspases and Bcl-2 family proteins, though the specific role of MOF in potentiating these effects requires further investigation through mechanistic studies including Western blotting for Raf/MAPK pathway inhibition and cellular uptake studies using confocal microscopy[8,10,11,37].

Moreover, the significant arrest of HepG2 cells in the G0-G1 phase reinforces the idea that SOR-MIL-53 interferes with cell cycle progression, potentially through the downregulation of cyclins and cyclin-dependent kinases (CDKs) necessary for the G1 to S phase transition[24,42]. This cell cycle blockade not only halts proliferation but also primes cells for apoptosis[43]. The reduction in S phase cells aligns with the suppressed DNA synthesis observed[44]which could further amplify the cytostatic and cytotoxic effects of SOR-MIL-53. The pronounced effects on HepG2 cells indicate a heightened sensitivity of liver cancer cells to SOR-MIL-53 treatment underscoring the dual mechanisms—apoptosis induction and cell cycle arrest—by which it exerts its anticancer activity. Future studies should extend apoptosis and cell cycle analysis to HCT-116 cells to validate consistency across cell lines and provide a more comprehensive understanding of the nanocomposite's mechanism of action.

Several limitations of the current study should be acknowledged: (1) The high variability in loading capacity indicates batch-to-batch reproducibility challenges that require optimization; (2) Release studies were conducted only at physiological pH, and acidic pH studies are needed to validate tumor-specific release; (3) Mechanistic studies including Western blotting for pathway analysis and confocal microscopy for cellular uptake are needed to elucidate the enhanced potency mechanisms; (4) Long-term stability studies and degradation product analysis are required to assess the safety profile of MOF degradation products; (5) The modest selectivity improvements indicate the need for active targeting strategies to achieve clinically relevant therapeutic windows.

Our findings are consistent with earlier studies on MOF-based drug delivery systems. For instance, it was very recently demonstrated the successful use of MOFs in delivering natural compounds like saponin (Alamdaran, Taheri-Kafrani, and Karimi 2024), highlighting the versatility of MOFs in carrying diverse therapeutic agents. The ability of MOFs to enhance the cytotoxic effects of sorafenib, as reflected in the reduced IC_{50} and enhanced entrapment efficiency, further emphasizes their potential as next-generation drug delivery platforms.

While MOF-based drug delivery for cancer treatment is well-documented[19,45,46]the specific application of MIL-53(Fe) for sorafenib delivery to both HCC and CRC represents a novel approach with potential clinical implications. The enhanced potency observed in this study, combined with the sustained release profile, suggests that MOF delivery could reduce dosing frequency and potentially minimize side effects. However, the modest selectivity improvements indicate that future research should focus on surface modification strategies, active targeting mechanisms, and stimuli-responsive release systems to achieve clinically meaningful therapeutic windows.

In conclusion, sorafenib loaded on MIL-53(Fe) offers an enhanced therapeutic strategy for treating HepG2 and HCT-116 cell lines, with improved potency and modest selectivity improvements compared to free sorafenib (Fig. 8). However, further studies, and in vivo investigations, are required to validate these findings and optimize MOF formulations for clinical applications. The development of MOF-based nanocarriers represents a significant advancement in addressing the challenges of conventional chemotherapy, particularly in enhancing drug solubility, potency and overcoming MDR.

Future prospects

The success of this study paves the way for exploring the use of MOFs in delivering other chemotherapeutic agents to a broader range of cancer types. Future research should focus on: (1) in vivo testing using animal models to validate efficacy and safety; (2) investigating long-term biocompatibility and degradation product toxicity; (3) elucidating the underlying molecular mechanisms through pathway analysis and cellular uptake studies; (4) optimizing MOF designs with surface modifications for active targeting to maximize drug delivery efficiency and selectivity; (5) developing stimuli-responsive release systems for tumor-specific drug delivery; (6) conducting pH-dependent release studies to validate tumor microenvironment-specific drug release mechanisms for clinical applications; and (7) characterization should include scanning electron microscopy (SEM) and transmission electron microscopy (TEM) imaging to provide detailed morphological information about particle shape, surface texture, and structural integrity of the MOF nanocomposites.

Conclusion

We conclude from the current study that MIL-53(Fe) MOF as a carrier is considered a promising nanocarrier for enhancing sorafenib potency as an anticancer agent. Loading sorafenib onto MOF demonstrated significant improvements in drug potency across cancer cell lines, with IC50 values decreasing from 12.58 ± 1.2 to 5.5 ± 0.6 μg/mL for HepG2 cells and from > 200 to 7.9 ± 0.8 μg/mL for HCT-116 cells after loading capacity correction. While selectivity improvements were observed (SI increased from 0.46 to 0.6 for HepG2 and from 0.2 to 0.42 for HCT-116), these values remain below the clinically relevant threshold of > 2, indicating that further optimization is needed to achieve meaningful therapeutic windows. The study successfully demonstrated sustained drug release over 48 h, high entrapment efficiency ($88.97\% \pm 3.2\%$), and significant induction of apoptosis and cell cycle arrest in HepG2 cells. However, batch-to-batch reproducibility challenges (LC variability of ± 11%) and the need for mechanistic studies, pH-responsive release validation, and active targeting strategies represent important areas for future research. Despite these limitations, the enhanced potency observed in both hepatocellular carcinoma and colorectal cancer cell lines suggests that MOF-based delivery systems hold promise for expanding sorafenib's therapeutic applications and overcoming limitations of conventional chemotherapy.

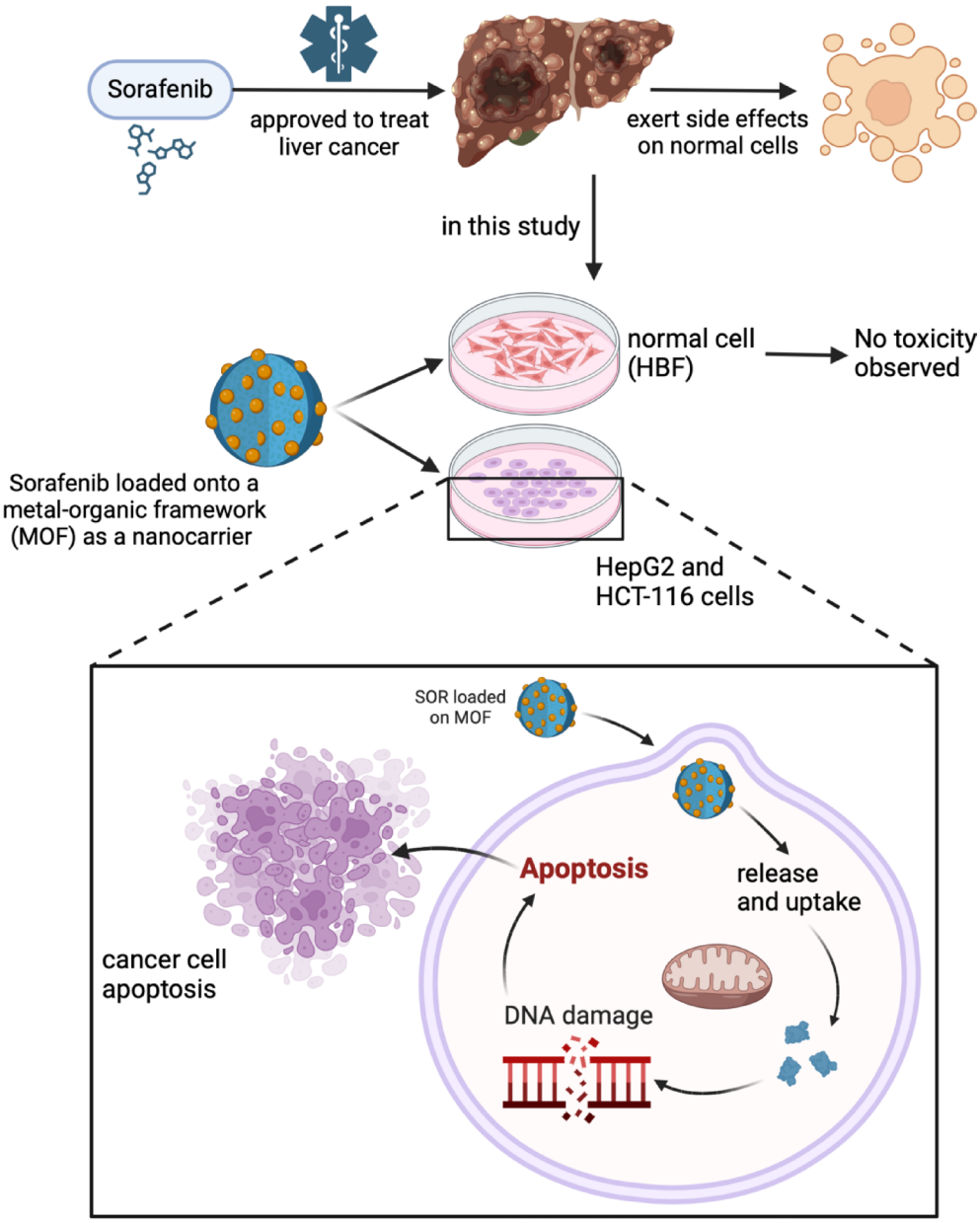

Fig. 8. Effectiveness of sorafenib-loaded MOFs (SOR-MIL-53) in enhancing anticancer activity against hepatocellular carcinoma (HepG2) and colorectal cancer (HCT-116) cell lines, with reduced toxicity observed in normal fibroblast cells (HFb-4).

Data availability

The data that support the findings of this study, including raw experimental data and gene expression data, are available from the corresponding authors [Prof. Dr. Emad Elzayat and Dr. Nourhan Hassan] upon reasonable request. The data were used during the research but are not publicly available due to privacy and institutional policy restrictions. Additional information regarding the study, including detailed protocols and statistical analyses, is also available upon reasonable request.

Received: 20 November 2024; Accepted: 19 August 2025
Published online: 18 September 2025

References

1. Bukowski, K., Kciuk, M. & Kontek, R. Mechanisms of multidrug resistance in cancer chemotherapy. *Int. J. Mol. Sci.* **21**, 3233 (2020).
2. Anwanwan, D., Singh, S. K., Singh, S., Saikam, V. & Singh, R. Challenges in liver cancer and possible treatment approaches. *Biochim. Et Biophys. Acta (BBA) - Reviews Cancer*. **1873**, 188314 (2020).

3. Shin, A. E., Giancotti, F. G. & Rustgi, A. K. Metastatic colorectal cancer: mechanisms and emerging therapeutics. *Trends Pharmacol. Sci.* **44**, 222–236 (2023).
4. Anand, U. et al. Cancer chemotherapy and beyond: current status, drug candidates, associated risks and progress in targeted therapeutics. *Genes Dis.* **10**, 1367–1401 (2023).
5. Wang, X., Zhang, H. & Chen, X. Drug resistance and combating drug resistance in cancer. *Cancer Drug Resist.* https://doi.org/10.20517/cdr.2019.10 (2019).
6. Chidambaram, M., Manavalan, R. & Kathiresan, K. Nanotherapeutics to overcome conventional cancer chemotherapy limitations. *J. Pharm. Pharm. Sci.* **14**, 67 (2011).
7. Sun, T. et al. Engineered nanoparticles for drug delivery in cancer therapy. *Angew. Chem. Int. Ed.* **53**, 12320–12364 (2014).
8. Voliotis, D. & Dumas, J. Clinical development of Sorafenib (BAY 43–9006) VEGFR and RAF inhibitor. in *Tumor Angiogenesis* 655–671 (Springer Berlin Heidelberg, Berlin, Heidelberg). https://doi.org/10.1007/978-3-540-33177-3_36
9. Ishihara, S. et al. Sorafenib inhibits vascular endothelial cell proliferation stimulated by anaplastic thyroid cancer cells regardless of BRAF mutation status. *Int. J. Oncol.* https://doi.org/10.3892/ijo.2019.4881 (2019).
10. Ramakrishnan, V. et al. Sorafenib, a dual Raf kinase/vascular endothelial growth factor receptor inhibitor has significant anti-myeloma activity and synergizes with common anti-myeloma drugs. *Oncogene* **29**, 1190–1202 (2010).
11. Liu, L. et al. Sorafenib blocks the RAF/MEK/ERK pathway, inhibits tumor angiogenesis, and induces tumor cell apoptosis in hepatocellular carcinoma model PLC/PRF/5. *Cancer Res.* **66**, 11851–11858 (2006).
12. Pang, Y. et al. Adverse events of Sorafenib in hepatocellular carcinoma treatment. *Am. J. Cancer Res.* **12**, 2770–2782 (2022).
13. Grossi, V. et al. Sorafenib inhibits p38α activity in colorectal cancer cells and synergizes with the DFG-in inhibitor SB202190 to increase apoptotic response. *Cancer Biol. Ther.* **13**, 1471–1481 (2012).
14. Singh, R. & Lillard, J. W. Nanoparticle-based targeted drug delivery. *Exp. Mol. Pathol.* **86**, 215–223 (2009).
15. Patra, J. K. et al. Nano based drug delivery systems: recent developments and future prospects. *J. Nanobiotechnol.* **16**, 71 (2018).
16. Taran, M., Safaei, M., Karimi, N. & Almasi, A. Benefits and application of nanotechnology in environmental science: an overview. *Biointerface Res. Appl. Chem.* **11**, 7860–7870 (2021).
17. Haleem, A., Javaid, M., Singh, R. P., Rab, S. & Suman, R. Applications of nanotechnology in medical field: a brief review. *Global Health J.* **7**, 70–77 (2023).
18. Butova, V. V., Soldatov, M. A., Guda, A. A., Lomachenko, K. A. & Lamberti, C. Metal-organic frameworks: structure, properties, methods of synthesis and characterization. *Rus. Chem. Rev.* **85**, 280–307 (2016).
19. He, S. et al. Metal-organic frameworks for advanced drug delivery. *Acta Pharm. Sin B.* **11**, 2362–2395 (2021).
20. Matsumura, Y. & Maeda, H. A new concept for macromolecular therapeutics in cancer chemotherapy: mechanism of tumoritropic accumulation of proteins and the antitumor agent Smancs. *Cancer Res.* **46**, 6387–6392 (1986).
21. Maranescu, B. & Visa, A. Applications of Metal-Organic frameworks as drug delivery systems. *Int. J. Mol. Sci.* **23**, 4458 (2022).
22. Sabzehmeidani, M. M. & Kazemzad, M. Recent advances in surface-mounted metal–organic framework thin film coatings for biomaterials and medical applications: a review. *Biomater. Res.* **27**, 115. https://doi.org/10.1186/s40824-023-00454-y (2023).
23. Zhang, Q. et al. Multi-Bioinspired MOF delivery systems from microfluidics for tumor multimodal therapy. *Adv. Sci. (Weinh).* **10**(33), e2303818. https://doi.org/10.1002/advs.202303818 (2023).
24. Li, H. et al. Doxorubicin-Loaded Metal-Organic framework nanoparticles as Acid-Activatable hydroxyl radical nanogenerators for enhanced chemo/chemodynamic synergistic therapy. *Materials* **15**, 1096 (2022).
25. Bray, F. et al. Global cancer statistics 2022: GLOBOCAN estimates of incidence and mortality worldwide for 36 cancers in 185 countries. *CA Cancer J. Clin.* **74**, 229–263 (2024).
26. Gao, T. et al. Exploring the pathogenesis of colorectal carcinoma complicated with hepatocellular carcinoma via microarray data analysis. *Front. Pharmacol.* **14**, 1201401. https://doi.org/10.3389/fphar.2023.1201401 (2023).
27. Duan, C. et al. Overcoming cancer Multi-drug resistance (MDR): reasons, mechanisms, nanotherapeutic solutions, and challenges. *Biomed. Pharmacother.* **162**, 114643 (2023).
28. Senapati, S., Mahanta, A. K., Kumar, S. & Maiti, P. Controlled drug delivery vehicles for cancer treatment and their performance. *Signal. Transduct. Target. Ther.* **3**, 7 (2018).
29. Colombo, M. Sorafenib in advanced hepatocellular carcinoma: A further step toward personalized therapy of liver cancer. *Gastroenterology* **136**, 1832–1835 (2009).
30. Chen, R. et al. Modulation of the tumour microenvironment in hepatocellular carcinoma by tyrosine kinase inhibitors: from modulation to combination therapy targeting the microenvironment. *Cancer Cell. Int.* **22**, 73 (2022).
31. Cheng, Y. et al. Synergistic anti-tumor efficacy of Sorafenib and Fluvastatin in hepatocellular carcinoma. *Oncotarget* **8**, 23265–23276 (2017).
32. Mao, W. et al. The important roles of RET, VEGFR2 and the RAF/MEK/ERK pathway in cancer treatment with Sorafenib. *Acta Pharmacol. Sin.* **33**, 1311–1318 (2012).
33. Fallah, A. et al. Therapeutic targeting of angiogenesis molecular pathways in angiogenesis-dependent diseases. *Biomed. Pharmacother.* **110**, 775–785 (2019).
34. Irawan, A., Prabowo, E., Riwanto, I. & Atmodjo, W. L. Anti-angiogenic effect of the combination of low-dose Sorafenib and EGCG in HCC-induced Wistar rats. *F1000Res* **11**, 289 (2022).
35. Fan, Q. et al. Research progress of Sorafenib drug delivery system in the treatment of hepatocellular carcinoma: an update. *Biomed. Pharmacother.* **177**, 117118 (2024).
36. Cai, M. et al. Metal organic frameworks as drug targeting delivery vehicles in the treatment of cancer. *Pharmaceutics* **12**, 232 (2020).
37. Shano, L. B., Karthikeyan, S., Kennedy, L. J., Chinnathambi, S. & Pandian, G. N. MOFs for next-generation cancer therapeutics through a biophysical approach—a review. *Front. Bioeng. Biotechnol.* **12**, 1397804. https://doi.org/10.3389/fbioe.2024.1397804 (2024).
38. Li, A., Yang, X. & Chen, J. A novel route to size-controlled MIL-53(Fe) metal–organic frameworks for combined chemodynamic therapy and chemotherapy for cancer. *RSC Adv.* **11**, 10540–10547 (2021).
39. Gordon, J., Kazemian, H. & Rohani, S. MIL-53(Fe), MIL-101, and SBA-15 porous materials: potential platforms for drug delivery. *Mater. Sci. Engineering: C.* **47**, 172–179 (2015).
40. Gao, W., Xiang, B., Meng, T. T., Liu, F. & Qi, X. R. Chemotherapeutic drug delivery to cancer cells using a combination of folate targeting and tumor microenvironment-sensitive polypeptides. *Biomaterials* **34**, 4137–4149 (2013).
41. Gyanani, V., Haley, J. C. & Goswami, R. Challenges of current anticancer treatment approaches with focus on liposomal drug delivery systems. *Pharmaceuticals* **14**, 835 (2021).
42. Zhao, H., Zhang, Y., Sun, J., Zhan, C. & Zhao, L. Raltitrexed inhibits HepG2 cell proliferation via G0/G1 cell cycle arrest. *Oncol. Res. Featuring Preclinical Clin. Cancer Ther.* **23**, 237–248 (2016).
43. Liu, Q. et al. Panduratin A inhibits cell proliferation by inducing G0/G1 phase cell cycle arrest and induces apoptosis in breast cancer cells. *Biomol. Ther. (Seoul).* **26**, 328–334 (2018).
44. Bugallo, A., Sánchez, M., Fernández-García, M. & Segurado, M. S-phase checkpoint prevents leading strand degradation from strand-associated nicks at stalled replication forks. *Nucleic Acids Res.* **52**, 5121–5137 (2024).
45. Elmehrath, S., Nguyen, H. L., Karam, S. M., Amin, A. & Greish, Y. E. BioMOF-Based Anti-Cancer drug delivery systems. *Nanomaterials* **13**, 953 (2023).

46. Guo, Z. et al. Metal–organic framework-based smart stimuli-responsive drug delivery systems for cancer therapy: advances, challenges, and future perspectives. *J. Nanobiotechnol.* **23**, 157 (2025).

Acknowledgements
The authors extend their appreciation to the University Higher Education Fund for funding this research work under the Research Support Program for Central Labs at King Khalid University through the project number CL/CO/A/5. The graphical abstract in the article was created with BioRender.com.

Author contributions
N.M.H. performed the experiments. E.M.E. and R.M. supervised the project. N.H. and N.M.H. wrote the first draft of the manuscript and prepared the figures. E.I. funded the project. E.M.E. conceived, coordinated, and supervised the study. All authors revised, reviewed, and commented on the manuscript.

Funding
The funding of this work is through Research Support Program for Central Labs at King Khalid University through the project number CL/CO/A/5.

Declarations

Competing interests
The authors declare no competing interests.

Ethics approval
Not applicable.

Consent for publication
Not applicable.

Consent to participate
Not applicable.

Additional information
Correspondence and requests for materials should be addressed to E.M.E. or N.H.

Reprints and permissions information is available at www.nature.com/reprints.

Publisher's note Springer Nature remains neutral with regard to jurisdictional claims in published maps and institutional affiliations.